Showcasing research from Professor Konkolewicz's laboratory, Department of Chemistry and Biochemistry, Miami University, Ohio, United States of America.

Dynamic polymer nanocomposites towards strain sensors and customizable resistors

Dynamic polymer materials with thermoresponsive dynamic covalent bonds were developed and reinforced with carbon nanotubes to create strong and flexible conductive materials. Tailoring the polymer microstructure for higher mechanical performance was a focus of the work. Carbon nanotubes reinforcement increased the mechanical strength of the networks, especially at higher strains. Taking advantage of the electrical conductivity of the carbon nanotubes allowed applications such as strain sensing. Finally, combining the dynamic polymer matrix to conductivity of the nanotubes allowed customizable resistors.

As featured in:

RSC Applied Polymers
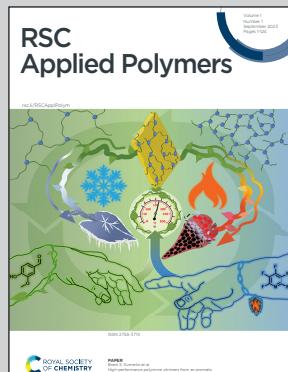
See Dominik Konkolewicz *et al.*, *RSC Appl. Polym.*, 2023, **1**, 30.

ROYAL SOCIETY OF **CHEMISTRY**

rsc.li/RSCApplPolym

PAPER

Check for updates

Dynamic polymer nanocomposites towards strain sensors and customizable resistors†

Obed J. Dodo, [ID] [a] Ibrahim O. Raji,[a] Ian J. Arny,[a] Camryn P. Myers,[a] Leilah Petit,[a] Kumari Walpita,[a] Derrick Dunn,[a] Carl J. Thrasher[b] and Dominik Konkolewicz [ID] *[a]

In the future, well-engineered and optimized flexible electronic devices will be woven into everyday accessories such as clothes, furniture, and healthcare monitoring devices. Herein, a series of multifunctional, flexible, conductive, and self-healing polymer nanocomposites that contribute to multiple electronic applications are reported. RAFT polymerization is employed in a modular approach to synthesize dynamic polymer nanocomposites (DPNs) using different architectures including interpenetrating (IPN) and block copolymer (BCN) networks through dynamic Diels−Alder and hydrogen bond cross-links. Structure−property relationships highlighting the impact of network architecture, chain-length, cross-link density, and carbon nanotubes loading are explored. Controlled addition of multiwalled carbon nanotubes (CNTs) as nano-reinforcements produces electrically conductive and mechanically enhanced DPNs with demonstrated application in the regulation of current flow towards a dimmable light emitting diode (LED). Further application of DPNs as strain sensors and customizable/tunable electrical resistors is demonstrated. Overall, this report furnishes new insights into designing next-generation custom resistors and materials for smart LED lighting.

Introduction

Dynamic polymer nanocomposites (DPNs) have potential applications in electronics and energy devices such as electronic skins, soft robots, flexible circuits, sensors, and energy harvesting devices due to their flexibility, low cost, facile processing, chemical resistance, and adjustable electrical properties.[1–8] Conventional electronic devices based on metal–oxide-semiconductor systems have limited mechanical flexibility, which presents challenges in this booming era of flexible and wearable electronics.[9–11] Owing to the inherent advantage of being light, healable, flexible, stretchable (>50% strain), DPNs have received attention, especially with demonstrated applications in soft robotics, human motion detection, personalized healthcare monitoring, and human machine interfaces.[12–15]

Introducing healability into polymeric electronic devices is appealing because functional self-healing materials enhance

the durability, toughness, of the system and reduce its maintanance.[8,16–18] Nevertheless, the dynamic chemistries that enable self-healing polymers[19,20] have received significantly more attention than intrinsically self-healing electronic and energy devices which restore device performance after damage.[21,22] Intrinsic self-healing in polymeric materials is enabled by supramolecular/noncovalent interactions or dynamic covalent bonds. Integrating these dynamic chemistries into polymers leads to materials with ability to undergo multiple reprocessing/repair cycles. In contrast, extrinsic self-healing polymers rely on interconnected vesicles or microcapsules of healing agents, giving a single-time healing upon damage to the material.[23] While progress has been made in extrinsically self-healing conductive composites, the single healing cycle limits their applications,[24,25] increasing the need for intrinsically dynamic conducting materials.

Exchange reactions involving reversible covalent and non-covalent bonds are advantageous in dynamic polymers and impart excellent bond strength and versatility. Dynamic covalent reactions include disulfide exchange, Diels–Alder (DA) cycloaddition, siloxane exchange, transesterification, thiol-Michael adduct exchange, [2 + 2] coumarin cycloaddition, and [4 + 4] anthracene cycloaddition.[20] Among non-covalent systems hydrogen (H) bonding is the most common non-covalent supramolecular interaction, resulting in highly dynamic polymers, since the weak interactions lead to viscoelastic materials with creep susceptibility but rapid self-

[a]*Department of Chemistry and Biochemistry, Miami University, 651 East High Street, Oxford, OH 45056, USA. E-mail: d.konkolewicz@miamioh.edu*
[b]*Department of Materials Science and Engineering, Massachusetts Institute of Technology, Cambridge, MA 02142, USA*

healing.[26] In contrast, dynamic covalent linkers are typically static, until an external stimulus is applied. Unique materials are possible by combining dynamic covalent and supramolecular linkers with dramatically different lifetimes.[26–28] These dynamic polymers have exciting properties such as self-healing and adaptability, however, they often have lower strength, and opto-electronic functionality compared to traditional electronic materials.[29]

To obtain simultaneous self-healing, enhanced mechanical properties, and electrical functionalities, conductive self-healing polymer composites have been developed by introducing conductive networks of nanomaterials into dynamic polymers.[29,30] Combining dynamic polymers with conductive nanomaterials (e.g., carbon nanomaterials and metallic fillers) results in a new class of bulk polymeric materials called DPNs. In DPNs, the nano-filler provides the electrical properties and mechanical reinforcement, and the polymer matrix harnesses dynamic exchange reactions to reconstruct damaged DPNs.[31]

For DPNs to function as electronic devices, the conductive nanofiller must surpass the percolation threshold, hence nanotubes or nanowires are preferred conductive fillers due to their rod like structure leading to interconnected conductive pathways.[22] Multiwalled carbon nanotubes (hereafter denoted as CNTs) or buckytubes are rolled up sheets of graphene forming nanoscale tubes featuring high aspect ratios greater than 10^3. These CNTs have extraordinary electrical conductivity, high mechanical strength, thermal conductivity, and high specific surface area (1.32×10^3 m^2 g^{-1}), making them excellent candidates in nanotechnology and sensing applications.[32,33] Since multiwalled CNTs provide the advantage of lower cost compared to the single walled alternatives, they are more suitable for cost-effective electronic devices and have received significant attention in literature.[31,34,35] CNT-enhanced DPNs have demonstrated healability, recyclability, conductivity, and thermoresponsive properties leading to applications in electromagnetic shielding, strain sensors, and electronic packaging materials.[36,37]

However, there remain key design and functionality challenges associated with DPNs including: [i] inefficient load transfer from the dynamic polymer matrix to the conductive filler, [ii] the trade-off between enhanced mechanical strength, dynamic properties, and material stretchability,[3,31,37] and [iii] demonstrating new electronic component applications. Challenge [i], the inefficient load transfer between CNT and the dynamic matrix is due to a lack of chemical interaction between conductive fillers and the polymer matrices. Poor transfer of load can lead to materials with inefficient reinforcement, or lower toughness. Prior attempts to solve this challenge pre-functionalized CNTs through harsh reactions.[38,39] Challenge [ii], the potential trade-offs between strength, dynamic properties, and stretchability is partly due to limited exploration of controlled and tailored polymer architecture explored for DPNs. Complex polymer architectures are needed for DPNs to demonstrate flexibility and stretchability even with the inclusion of a conductive nanofiller.[35] Challenge [iii], developing new functionalities beyond sensing, dielectric

actuators, field-effect transistors, and stretchable conductors is still challenging, in part because of challenges in material design.[22] Overall, this work provides enhanced structure property relationships between dynamic polymer networks and CNT-DPN mechanical and electrical performance, resulting in progress towards solving challenges [i], [ii], and [iii].

When designing DPNs, the choice of polymer architecture contributes significantly to the overall thermomechanical properties of materials.[40] Key polymer architectural features such as cross-link density, chain length, cross-link distribution, topology, and orientation of polymer networks impact properties such as material strength, phase transition temperatures, stress relaxation, creep, and elongation at break. The relationship between polymer architecture and the properties of DPNs is underexplored,[41,42] especially in dynamic polymer composite systems. Due to the limited studies correlating network architecture to materials properties, and inefficient load transfer between reinforcement and matrix, it is critical to develop reliable approaches towards DPN composites which can be tuned by polymer and network architecture. Determining how network architecture impacts DPN properties will provide new insights into designing highly functional materials with advanced properties.[42]

In a previous study, we demonstrated a method for macromolecular engineered nano reinforcement in linear and branched polymers using CNT as a nanofiller to achieve bulk DPNs. This system used the bonding of furan to the CNT surface through Diels–Alder chemistry to transfer load between reinforcement and matrix,[31] however the DPNs had limited functionality. This led to a subsequent development of DPNs containing three types of dynamic bonds with distinct roles, resulting in recyclable DPNs with better elongation and higher electrical conductivity.[35] Results from that study not only confirmed the synergy of dynamic bonds, but also highlighted the potential interplay of dynamic bonds and primary chain structure on advanced materials properties. However, there is still no comprehensive study that connects the network architecture of polymers to their corresponding composite material's electrical and mechanical properties, significantly limiting the functionalities and high-performance applications of DPNs.[42]

Here, we present an advanced category of DPNs with inherent ability to modify the surface of CNTs under mild conditions, without requiring pre-functionalization.[43] The approach results in effective reinforcement of mechanical strength without stretchability trade-off, and meaningful electrical conductivity. Findings in this contribution enabled application of CNT composites as customizable resistors and a strain sensing device. This work presents a detailed structure–property study of the impact of network architecture, cross-link density, cross-link distribution, chain length, and polymer microstructure on the mechanical and electrical performance of CNT composite DPNs. While there are numerous reports on healable DPNs for strain sensing applications, to the best of our knowledge, this is the first demonstration of DPNs (with inherent conductivity) as customizable/tunable resistors

© 2023 The Author(s). Published by the Royal Society of Chemistry

RSC Appl. Polym., 2023, 1, 30–45 | 31

enabled through self-healing and an electrically conductive nanofiller. More broadly, the extensive structure–property study, and simple approach to allow load transfer from the filler to reinforcement, can guide future DPN composites towards new applications in challenging environments.

Results and discussion

CNT reinforced DPN enabled by macromolecular engineering

Reversible addition fragmentation chain transfer (RAFT)[44] polymerization was used as a reversible deactivation radical polymerization (RDRP)[45] technique to synthesize well-defined acrylate-based polymers with the main polymer chain comprising of ethyl acrylate (EA). Scheme 1 gives the polymer architectures and dynamic properties of the materials. Scheme 1A shows the structure of dynamic UPy and FMA linkers and the ranges of dynamic polymer architectures. Scheme 1B gives the dynamic crosslinks between UPy units, furan–maleimide bonds, and dynamic interactions between the CNT surface and the furan unit. Scheme 1C and D show the BCN synthesis and dynamic exchange for IPN and BCN type materials respectively. Scheme 1E shows the non-dynamic GMA linker after ring opening of the epoxide with ethylene diamine and its non-dynamic nature. The GMA based control materials is non-dynamic and also unable to bind to the CNTs. This way the GMA based materials can identifying the impact of Diels–Alder chemistry on the load transfer between the reinforcement and matrix and dynamic exchange within the network.

Various formulations of dynamic polymers (Table 1) confirmed by ^{1}H NMR and GPC (Table S1†) were used to develop a novel class of DPNs. In general, the synthesized polymers have well controlled molecular weight distributions, with number averaged molecular weight (M_n) close to the theoretical value and dispersity ($Đ$) below 1.4. In the case of the block copolymers, the final block copolymer has a M_n comparable to the theoretical M_n, with positive shifts in molecular weight upon each chain extension. However, since the final block only constituted a small increase in total molecular weight, the shift upon the third chain extension was relatively small.

Subsequently, a facile approach was used to prepare DPNs through solution processing of dynamic polymers with CNTs using ultrasonication. Covalent bonding between polymer chains and CNTs was achieved through the intrinsic Diels–Alder chemistry,[31,43] without the need for pre-functionalization or post-polymerization modification. Integration of 2-ureido-4 [1H]-pyrimidinone (UPy) and furfuryl-methacrylate (FMA) motifs enabled dynamic supramolecular H-bonding through dimerized quadrupole H-bond interactions and dynamic covalent DA cross-links respectively (Scheme 1). Multiple dynamic polymer structures were explored to study the impact of network architecture in nanoreinforced conductive composites. Specific thermomechanical properties studied include T_g, strain at break (ε_{break}), peak stress (σ_{peak}), and Young's modulus (Y) as outlined in Table 1 and Table S2.†[42] Pendant furan groups on FMA were leveraged as a diene on polymer

side chains and cross-linked using 1,1′-(methylene-di-4,1-phenyl-ene)bismaleimide (BMI) through a reversible [4 + 2] DA cycloaddition reaction. About $\frac{1}{2}$ mole equivalent of BMI was used to cross-link 1 mole equivalent of FMA motifs through dynamic covalent DA chemistry. Since commercial BMI is ∼95% pure,[46] consistent with findings reported by Bai et al.,[47] previous reports showed that the small amount of unreacted FMA motifs have the ability to engage in DA chemistry through FMA furan groups on polymer chains with π-bonds on CNTs acting as dienophiles.[31,35]

To study the impact of network architecture on DPNs, interpenetrating polymer networks (IPNs) and tri-block copolymer networks (BCNs) were synthesized resulting in DPN entries 1–5 and 6–8 in Table 1 respectively. Designations IPN-Lin$_w$UPy$_x$FMA$_y$ and BCN-Blk$_w$UPy$_x$FMA$_y$ are used to describe IPN and BCN-based DPNs in this study respectively. Lin$_w$ represents a linear polymer chain with w number of EA units, BCN-Blk$_w$ represents a tri-block polymer chain with w number of EA units, while x and y represent the number of UPy and FMA units respectively. Eight different polymers were studied with CNT loadings ranging from 0, 0.5, 1, to 2.5 wt% leading to the comprehensive entries in Table 1. To confirm the significance of FMA bonding to the CNT surface, control materials were developed without furan group that can bind to the CNT surface through Diels–Alder chemistry. A BCN was developed where only the H-bonding UPy units were used, in entries 13 and 14 of Table 1. Similarly, the epoxide containing GMA replaced FMA in BCN 17 and 18 respectively, which serves as an important control, since the crosslinked epoxy chemistry derived from GMA cannot bind to the CNT surface through Diels–Alder chemistry.

Herein, we successfully validate the multifunctionality of DPNs in electrical circuits, demonstrating their ability to function as on-demand tunable electronic devices for custom resistors with ability to also act as semiconductors without the need for switching their electronic capacity unlike traditional memory resistors.[48] This work hence contributes to the fast-growing field of healable electronic devices with new insight on tailoring the electronic properties of advanced conductive polymers.

Structure–property relationships in macromolecular engineered DPNs

Material characterization. Material characterization was accomplished using dynamic mechanical analysis, thermogravimetric analysis, differential scanning calorimetry, infrared spectroscopy (IR), scanning electron microscopy, and tensile testing. DPNs with IPN architecture include IPN-Lin$_{100}$UPy$_5$FMA$_5$ (with equal 5 mol% FMA and UPy cross-links), higher cross-linked IPN-Lin$_{100}$UPy$_{7.5}$FMA$_{7.5}$ (with equal 7.5 mol% FMA and UPy cross-link), IPN-Lin$_{100}$UPy$_{7.5}$FMA$_{15}$ (with 7.5 mol% UPy and double FMA equivalent cross-link), IPN-Lin$_{100}$UPy$_{15}$FMA$_{7.5}$ (with 7.5 mol% FMA and double UPy equivalent cross-link), and longer chain-length IPN-Lin$_{150}$UPy$_{11.25}$FMA$_{11.25}$ (with equal 7.5 mol% FMA and UPy cross-link density) (Fig. 1A–C). Synthesis of linear poly
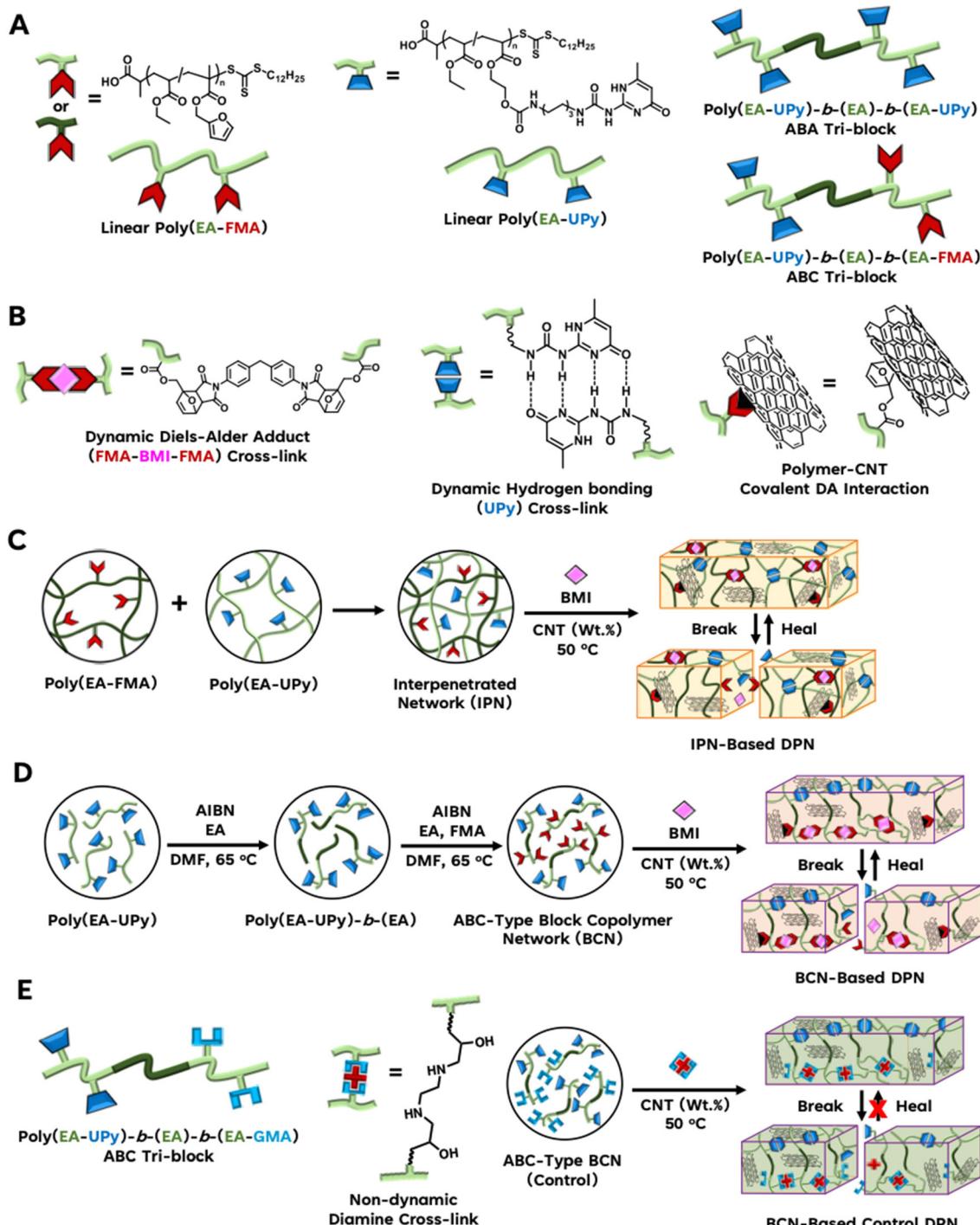
Scheme 1 DPN synthesis enabled by macromolecular engineering of dynamic polymer networks with CNTs. (A) Legends describing the dynamic polymer network architecture. (B) dynamic non-covalent hydrogen bonding and covalent Diels−Alder interaction between polymer chains and/or CNT nanofiller. (C) Synthesis of IPN-based DPN materials through the combination of interpenetrated linear poly(EA-FMA) and linear poly(EA-UPy). (D) Synthesis of BCN-based DPNs by chain extension of linear poly(EA-UPy) to obtain poly(EA-UPy)-*b*-(EA) which was further chain extended to obtain poly(EA-UPy)-*b*-(EA)-*b*-(EA-FMA) tri-block DPN. (E) Poly(EA-UPy)-*b*-(EA)-*b*-(EA-GMA) control polymer and its synthesis into material without dynamic furan-CNT interactions. All DPN polymer compositions are outlined in Table 1.

(EA-FMA) and poly(EA-UPy) are provided in Scheme S1.† DPNs based on BCN architecture include BCN-Blk$_{100}$UPy$_{7.5}$ (ABA-type block copolymer with a total of 7.5 mol% UPy cross-link),

BCN-Blk$_{100}$UPy$_{3.75}$FMA$_{3.75}$ (ABC-type block copolymer with 7.5 mol% UPy and FMA cross-link), and control material BCN-Blk$_{100}$UPy$_{3.75}$GMA$_{3.75}$ (ABC-type block copolymer with

Table 1 DPN formulations with corresponding mechanical and conductivity properties

Entry	Polymers	CNT wt%	DPN designation	ε_{break} [%]	σ_{peak} [MPa]	Y [MPa]	κ^a S cm^{-1}
1	Poly[EA$_{100}$-UPy$_5$] & poly[EA$_{100}$-FMA$_5$]	0	IPN-Lin$_{100}$UPy$_5$FMA$_5$0%CNT	169 ± 05	0.237 ± 0.009	0.3 ± 0.1	—
2	Poly[EA$_{100}$-UPy$_5$] & poly[EA$_{100}$-FMA$_5$]	0.5	IPN-Lin$_{100}$UPy$_5$FMA$_5$0.5%CNT	164 ± 05	0.31 ± 0.03	0.45 ± 0.03	—
3	Poly[EA$_{100}$-UPy$_5$] & poly[EA$_{100}$-FMA$_5$]	1	IPN-Lin$_{100}$UPy$_5$FMA$_5$1%CNT	150 ± 20	0.61 ± 0.03	0.74 ± 0.04	0.038 ± 0.005
4	Poly[EA$_{100}$-UPy$_{7.5}$] & poly[EA$_{100}$-FMA$_{7.5}$]	0	IPN-Lin$_{100}$UPy$_{7.5}$FMA$_{7.5}$0%CNT	110 ± 20	1.64 ± 0.04	3.3 ± 0.3	—
5	Poly[EA$_{100}$-UPy$_{7.5}$] & poly[EA$_{100}$-FMA$_{7.5}$]	1	IPN-Lin$_{100}$UPy$_{7.5}$FMA$_{7.5}$1%CNT	70 ± 10	3.2 ± 0.2	7.9 ± 0.5	0.134 ± 0.027
6	Poly[EA$_{100}$-UPy$_{7.5}$] & poly[EA$_{100}$-FMA$_{7.5}$]	2.5	IPN-Lin$_{100}$UPy$_{7.5}$FMA$_{7.5}$2.5%CNT	71 ± 0.1	5.8 ± 0.2	14.6 ± 0.2	0.400 ± 0.005
7	Poly[EA$_{100}$-UPy$_{7.5}$] & double poly[EA$_{100}$-FMA$_{7.5}$]	0	IPN-Lin$_{100}$UPy$_{7.5}$FMA$_{15}$0%CNT	110 ± 10	3.16 ± 0.03	5.3 ± 0.4	—
8	Poly[EA$_{100}$-UPy$_{7.5}$] & double poly[EA$_{100}$-FMA$_{7.5}$]	1	IPN-Lin$_{100}$UPy$_{7.5}$FMA$_{15}$1%CNT	90 ± 10	4 ± 1	8.1 ± 0.6	0.09 ± 0.01
9	Double poly[EA$_{100}$-UPy$_{7.5}$] & poly[EA$_{100}$-FMA$_{7.5}$]	0	IPN-Lin$_{100}$UPy$_{15}$FMA$_{7.5}$0%CNT	128 ± 02	2.46 ± 0.07	3.3 ± 0.1	—
10	Double poly[EA$_{100}$-UPy$_{7.5}$] & poly[EA$_{100}$-FMA$_{7.5}$]	1	IPN-Lin$_{100}$UPy$_{15}$FMA$_{7.5}$1%CNT	99 ± 05	2.87 ± 0.07	5.9 ± 0.2	0.059 ± 0.004
11	Poly[EA$_{150}$-UPy$_{11.25}$] & poly[EA$_{150}$-FMA$_{11.25}$]	0	IPN-Lin$_{150}$UPy$_{11.25}$FMA$_{11.25}$0%CNT	50.5 ± 0.5	5.5 ± 0.3	22 ± 2	—
12	Poly[EA$_{150}$-UPy$_{11.25}$] & poly[EA$_{150}$-FMA$_{11.25}$]	1	IPN-Lin$_{150}$UPy$_{11.25}$FMA$_{11.25}$1%CNT	50 ± 1	8.0 ± 0.9	31.5 ± 2	0.125 ± 0.007
13	Poly[(EA$_{20}$-UPy$_{3.75}$)-b-(EA$_{20}$-UPy$_{3.75}$)]	0	BCN-Blk$_{100}$UPy$_{7.5}$0%CNT	100 ± 10	2.28 ± 0.02	4.7 ± 0.2	—
14	Poly[(EA$_{20}$-UPy$_{3.75}$)-b-(EA$_{20}$-UPy$_{3.75}$)]	1	BCN-Blk$_{100}$UPy$_{7.5}$1%CNT	83 ± 03	2.69 ± 0.03	5.3 ± 0.8	0.027 ± 0.001
15	Poly[(EA$_{20}$-UPy$_{3.75}$)-b-(EA$_{20}$-FMA$_{3.75}$)]	0	BCN-Blk$_{100}$UPy$_{3.75}$FMA$_{3.75}$0%CNT	85.6 ± 0.5	3.9 ± 0.2	5.9 ± 0.2	—
16	Poly[(EA$_{20}$-UPy$_{3.75}$)-b-(EA$_{20}$-FMA$_{3.75}$)]	1	BCN-Blk$_{100}$UPy$_{3.75}$FMA$_{3.75}$1%CNT	74 ± 03	5.94 ± 0.04	12.1 ± 0.1	0.07 ± 0.01
17	Poly[(EA$_{20}$-UPy$_{3.75}$)-b-(EA$_{20}$-GMA$_{3.75}$)]	0	BCN-Blk$_{100}$UPy$_{3.75}$GMA$_{3.75}$0%CNT	84 ± 04	5.90 ± 0.03	9.6 ± 0.2	—
18	Poly[(EA$_{20}$-UPy$_{3.75}$)-b-(EA$_{20}$-GMA$_{3.75}$)]	1	BCN-Blk$_{100}$UPy$_{3.75}$GMA$_{3.75}$1%CNT	86 ± 02	6.6 ± 0.3	12.2 ± 0.2	0.039 ± 0.001

^{a} Where — is given for conductivity (κ) no measurement could be made with the instrumentation.

7.5 mol% UPy and GMA cross-link) (Scheme S2† and Table 1). Glycidyl methacrylate (GMA) was used in BCN-Blk$_{100}$UPy$_{3.75}$GMA$_{3.75}$ as a control for FMA, resulting in replacement of pendant furan with epoxy group on the polymer side chain. GMA cross-linking was achieved using N,N'-dimethylethylenediamine through epoxy ring-opening reaction (Scheme S3† and Scheme 1E).

Relatively low glass transition temperatures (T_g) below room temperature (−7.1 to +3.4 °C) were obtained for all DPNs. The low T_g arises from EA, with an uncrosslinked T_g of −24 °C,[49] being the major component of each of the materials, facilitating dynamic behavior.[50] Fig. S3(A)† gives the full IR spectrum of unreinforced bulk IPN-Lin$_{100}$UPy$_{7.5}$FMA$_{7.5}$0%CNT and reinforced IPN-Lin$_{100}$UPy$_{7.5}$FMA$_{7.5}$1%CNT with the proposed characterization outlined in Table S3† and a closer look at the spectra is provided in Fig. S4,† confirming the functional groups present. Additionally, a DSC trace used to estimate the T_g of materials is provided in Fig. S3(B)† using a BCN-Blk$_{100}$UPy$_{7.5}$0%CNT sample as a typical example.

Dynamic mechanical analysis. Initially, dynamic mechanical, and thermal properties of DPNs were considered. Fig. 1(A–C) gives a depiction of architectural changes adapted in IPN-Lin$_{100}$UPy$_{7.5}$FMA$_{7.5}$, IPN-Lin$_{100}$UPy$_{7.5}$FMA$_{15}$, and IPN-Lin$_{100}$UPy$_{15}$FMA$_{7.5}$ without CNT. Frequency sweep analysis compares all three materials to gain insight into how difference in architectural features impacts dynamic properties. In all cases the storage modulus (E') is above the loss modulus (E''), indicating viscoelastic materials with the solid like properties dominating over loss properties at all frequencies, and moduli are in the order of MPa. This is in contrast to earlier studies where the purely UPy crosslinked polymer networks substantially had lower moduli in the order of 10 kPa, and a clear crossover to viscoelastic liquid behavior at timescales of 10–100 s.[40]

Presence of 1 wt% CNT in IPN-Lin$_{100}$UPy$_{7.5}$FMA$_{7.5}$ gave a substantial increase in the storage modulus (E') of IPN-Lin$_{100}$UPy$_{7.5}$FMA$_{7.5}$1%CNT compared to unreinforced IPN-Lin$_{100}$UPy$_{7.5}$FMA$_{7.5}$ 0%CNT (dark and light purple circles in Fig. 1A), this can be attributed to the presence of CNT as effective nanoreinforcements and an equal molar amount of DA and UPy cross-linked IPN networks. Doubling the amount of DA cross-linked networks as is the case with IPN-Lin$_{100}$UPy$_{7.5}$FMA$_{15}$ resulted in a slightly higher E' compared to the unreinforced IPN-Lin$_{100}$UPy$_{7.5}$FMA$_{7.5}$, (Fig. 1A dark and light orange circles). This suggests that DA cross-links largely contributes to the modulus of the IPN-Lin$_{100}$UPy$_{7.5}$FMA$_{15}$ materials such that addition of only 1 wt% CNT does not significantly change the E'. The smaller measured reinforcement in IPN-Lin$_{100}$UPy$_{7.5}$FMA$_{15}$ compared to IPN-Lin$_{100}$UPy$_{7.5}$FMA$_{7.5}$ could be due to a more uniform network in IPN-Lin$_{100}$UPy$_{7.5}$FMA$_{7.5}$.

IPN-Lin$_{100}$UPy$_{7.5}$FMA$_{15}$ materials had higher modulus compared to IPN-Lin$_{100}$UPy$_{15}$FMA$_{7.5}$ (Fig. 1A). This has been observed in prior work,[40] where higher loadings of UPy containing polymers, compared to dynamic covalent polymers, leads to overall lower moduli, presumably due to weaker linkages in the network. Additionally, due to the lower loading
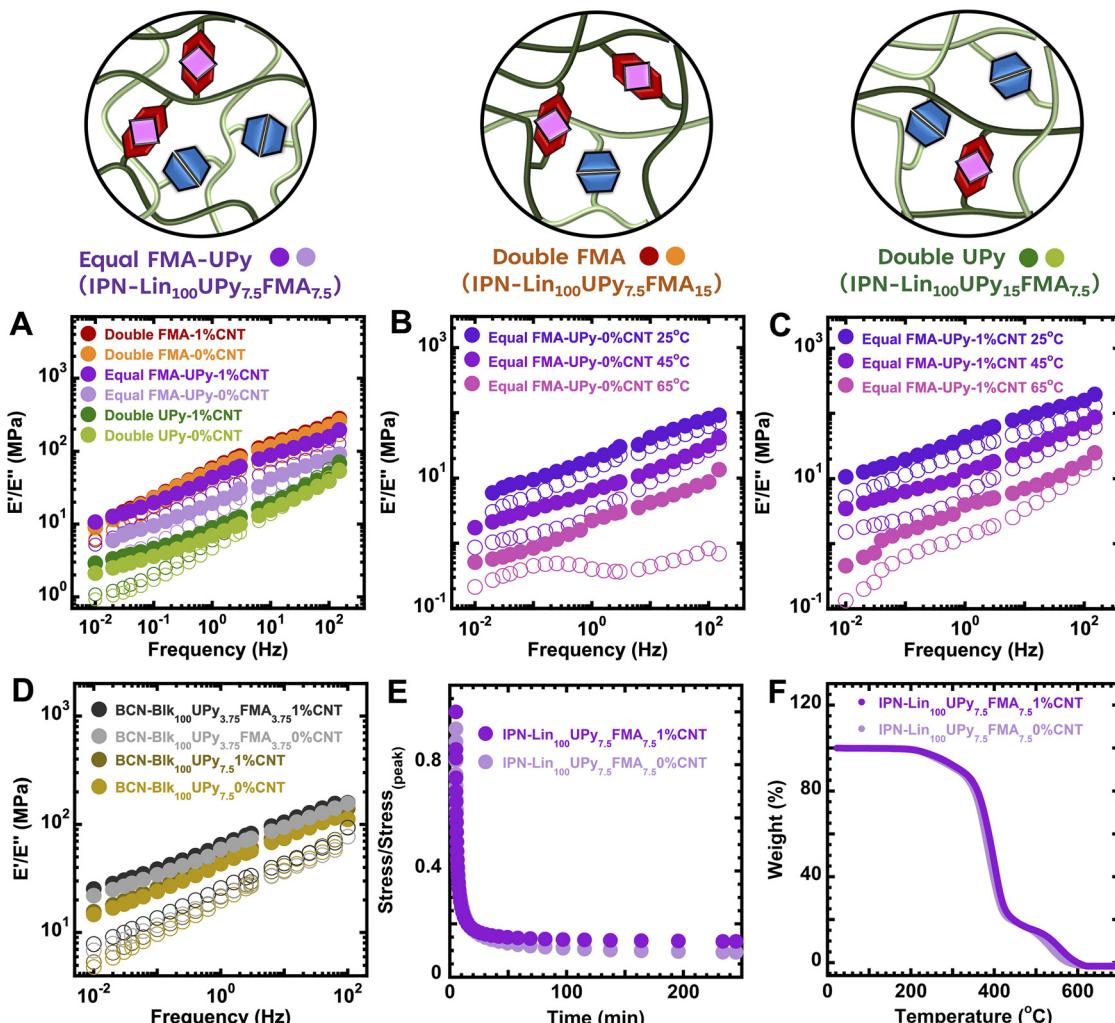
Fig. 1 Architecture and composition of unreinforced IPN–Lin$_{100}$UPy$_{7.5}$FMA$_{7.5}$, IPN–Lin$_{100}$UPy$_{7.5}$FMA$_{15}$, and IPN–Lin$_{100}$UPy$_{15}$FMA$_{7.5}$ are provided. In frequency sweeps, solid points represent E' and hollow points represent E''. Dynamic and thermal properties of DPNs in this study include: (A) combined frequency sweeps of unreinforced and reinforced IPN–Lin$_{100}$UPy$_{7.5}$FMA$_{7.5}$, IPN–Lin$_{100}$UPy$_{7.5}$FMA$_{15}$, and IPN–Lin$_{100}$UPy$_{15}$FMA$_{7.5}$ at 25 °C. (B) Combined frequency sweeps of unreinforced IPN–Lin$_{100}$UPy$_{7.5}$FMA$_{7.5}$ at different temperatures of 25, 45, and 65 °C. (C) Combined frequency sweeps of 1%CNT reinforced IPN–Lin$_{100}$UPy$_{7.5}$FMA$_{7.5}$ at different temperatures of 25, 45, and 65 °C. (D) Combined frequency sweeps of unreinforced and reinforced BCN-Blk$_{100}$UPy$_{7.5}$ and BCN-Blk$_{100}$UPy$_{3.75}$FMA$_{3.75}$ at 25 °C. (E) Stress relaxations and (F) typical TGA trace of reinforced and unreinforced IPN–Lin$_{100}$UPy$_{7.5}$FMA$_{7.5}$ materials. Colored and hollow circles represent storage and loss modulus respectively in (A–D).

of FMA units, the IPN–Lin$_{100}$UPy$_{15}$FMA$_{7.5}$ material as fewer opportunities for effective bonding between the matrix and CNTs.

Overall, IPN–Lin$_{100}$UPy$_{7.5}$FMA$_{7.5}$ which contains an equal mol% of FMA and UPy cross-links stands out in Fig. 1A, with the most significant increase in E' upon addition of 1% of CNTs. This could be in part due to the material with equimolar UPy and FMA polymer giving a more uniform network than when an excess of the FMA or UPy based linker is used. This indicates that true reinforcement without trade-offs in dynamic property of DPNs was achieved by using an equimolar amount of DA and UPy cross-linking, making IPN–Lin$_{100}$UPy$_{7.5}$FMA$_{7.5}$ an excellent material for further studies.

Fig. 1(B and C) reveals the impact of temperature on frequency sweep traces of unreinforced IPN–Lin$_{100}$UPy$_{7.5}$FMA$_{7.5}$0% CNT and reinforced IPN–Lin$_{100}$UPy$_{7.5}$FMA$_{7.5}$1%CNT respectively.

Higher temperatures decreased the E' of IPN–Lin$_{100}$UPy$_{7.5}$FMA$_{7.5}$, suggesting a pattern of thermoresponsive behavior due to partial dissociation of Diels–Alder units, which was present both with and without 1% of CNTs.[35] Furthermore, triblock-based BCN-Blk$_{100}$-UPy$_{7.5}$ and BCN-Blk$_{100}$UPy$_{3.75}$FMA$_{3.75}$ gave comparable E', although BCN-Blk$_{100}$UPy$_{3.75}$FMA$_{3.75}$ materials had higher E' upon CNT reinforcement as shown in Fig. 1D. In the case of BCN-based DPN materials in Fig. 1D, DA containing BCN-Blk$_{100}$UPy$_{3.75}$FMA$_{3.75}$ gave higher E' (dark and light blue circles in Fig. 1D) compared to BCN-Blk$_{100}$-UPy$_{7.5}$ which only contains UPy cross-links as shown in Scheme S2(C).† This further supports the previous suggestion that DA cross-links contribute significantly to material's modulus, due to effectively permanent linkers at ambient temperature.

Importantly, $BCN-Blk_{100}-UPy_{7.5}$ materials can be considered as control systems because they do not contain any FMA-based DA cross-links and as such showed minimal difference between the frequency sweep of the reinforced and unreinforced variants. This is likely due to no possibility for DA bonding between CNT and $BCN-Blk_{100}-UPy_{7.5}$. $BCN-Blk_{100}UPy_{3.75}FMA_{3.75}1\%CNT$ had only a small increase in in E' compared to the unreinforced variants $BCN-Blk_{100}UPy_{3.75}FMA_{3.75}0\%CNT$ (Fig. 1D), which again could be due to lower network uniformity in the system with blocky DA units. This further highlights $IPN-Lin_{100}UPy_{7.5}FMA_{7.5}$ materials as candidates for further studies. Stress-relaxation experiments of $IPN-Lin_{100}UPy_{7.5}FMA_{7.5}$ revealed ~90% stress relaxation with time (Fig. 1E) indicating their potential for energy absorbing applications.[51] Addition of 1 wt% CNT nanoreinforcement only caused a slight reduction in the stress relaxation capabilities of $IPN-Lin_{100}UPy_{7.5}FMA_{7.5}1\%CNT$. Prior work showed that IPN dynamic materials crosslinked with FMA-BMI and UPy linkers maintain permanent shape fidelity from the essentially static Diels–Alder linkers, despite their excellent stress relaxation which occurs through exchange of UPy linkers.[52]

Degradation temperatures T_d of $IPN-Lin_{100}UPy_{7.5}FMA_{7.5}$ were in the range of 300–400 °C (Fig. 1F) similar to the T_d of other poly(EA)-based materials reported in literature.[31,35] Addition of CNT as nanofillers had no significant impact on the stress relaxation and T_d of $IPN-Lin_{100}UPy_{7.5}FMA_{7.5}$, presumably due to the small fraction of nanofiller added, and the thermoreversibility of the Diels–Alder bonds between the matrix and CNT.

Impact of CNT loading and polymer architecture on DPNs.
Unlike DMA, which is performed at low strain (<5%) to be within the linear viscoelastic regime, the impact of CNT reinforcement is likely to be most significant at higher strains, where the mechanical loads are substantially larger. Architectural features and corresponding stress–strain tensile test results of IPN-based $IPN-Lin_{100}UPy_{7.5}FMA_{7.5}$, $IPN-Lin_{100}UPy_{7.5}FMA_{15}$, and $IPN-Lin_{100}UPy_{15}FMA_{7.5}$ are shown in Fig. 2(A–C). Likewise, architectural features and corresponding mechanical properties of BCN-based $BCN-Blk_{100}-UPy_{7.5}$, $BCN-Blk_{100}UPy_{3.75}FMA_{3.75}$, and $BCN-Blk_{100}UPy_{3.75}GMA_{3.75}$, are shown in Fig. 2(D–F).

The impact of CNT loading is considered in Fig. 2A showing a progressive rise in peak stress (σ_{peak}) as CNT loading increases in $IPN-Lin_{100}UPy_{7.5}FMA_{7.5}$. σ_{peak} increased by ~100% upon the addition of 1% CNTs and by 250% upon the addition of 2.5% CNTs. Addition of CNT nanofillers led to a slight decrease in material strain; however, self-healing was achieved in all materials under thermal stimulus of 90 °C for up to 24 hours (Fig. 3B). A similar trend is also observed in Fig. S3(C)† with less cross-linked $IPN-Lin_{100}UPy_5FMA_5$ containing 5 mol% cross-link density. Double DA cross-linked $IPN-Lin_{100}UPy_{7.5}FMA_{15}1\%CNT$ gave a 27% increase in σ_{peak} compared to the unreinforced $IPN-Lin_{100}UPy_{7.5}FMA_{7.5}0\%CNT$ as shown in Fig. 2B and Table 1. This is most likely due to the presence of more covalent DA cross-links in

$IPN-Lin_{100}UPy_{7.5}FMA_{15}$, increasing the 0% CNT material's strength. This is consistent with Fig. 1 where DA cross-links were found to significantly contribute to material modulus, with a smaller impact of CNT reinforcement. Fig. 2C shows that doubling the H-bond cross-links compared to DA cross-links resulted in lower mechanical strength of $IPN-Lin_{100}UPy_{15}FMA_{7.5}$ compared to $IPN-Lin_{100}UPy_{7.5}FMA_{7.5}$ and $IPN-Lin_{100}UPy_{7.5}FMA_{15}$ (Fig. 2A and B). However, the presence of more H-bonds gave better healing efficiency as shown in the time evolution healing of $IPN-Lin_{100}UPy_{15}FMA_{7.5}$ where healing properties of the materials can be as shown in Fig. S3(D and E),† further confirming thermoresponsive behavior.[35,53] Consistent with the DMA data in Fig. 1A, there is minimal reinforcement of $IPN-Lin_{100}UPy_{15}FMA_{7.5}$ upon the addition of 1% CNTs.

To better understand the impact of architecture on the mechanical properties of DPNs, different crosslink densities and chain lengths were studied. The lower density of crosslinks in $IPN-Lin_{100}UPy_5FMA_51\%CNT$ gave a σ_{peak} of 0.61 ± 0.03 MPa resulted in ~25% of the peak stress of 7.5 mol% cross-linked $IPN-Lin_{100}UPy_{7.5}FMA_{7.5}1\%CNT$ with a σ_{peak} of 3.2 ± 0.2 MPa (Fig. S3(C)† and Fig. 2A). This aligns with previous reports that suggest enhanced mechanical performance increases with cross-link density.[33,35] Longer-chain variant $IPN-Lin_{150}UPy_{11.25}FMA_{11.25}1\%CNT$ with a σ_{peak} of 8 ± 0.9 MPa and 150 EA units resulted in an impressive ~2.5-fold increase in stress compared to shorter-chain $IPN-Lin_{100}UPy_{7.5}FMA_{7.5}1\%CNT$ with only 3.2 ± 0.2 MPa σ_{peak} and 100 EA units (Fig. S3(F)† and Fig. 2A). This is attributed to the longer chains having more elastically effective crosslinks, increased number of entanglements, and effective interactions with the CNT nanofiller.

Furthermore, to explore the impact of architecture on DPN performance, tri-block $BCN-Blk_{100}UPy_{7.5}$, $BCN-Blk_{100}UPy_{3.75}FMA_{3.75}$, and $BCN-Blk_{100}UPy_{3.75}GMA_{3.75}$ were studied. Integration of only UPy units into $BCN-Blk_{100}UPy_{7.5}$ resulted in relatively similar outcomes when compared to double UPy containing $IPN-Lin_{100}UPy_{15}FMA_{7.5}$. This includes high self-healing efficiencies, ≤17% increase in σ_{peak} on addition of 1 wt% CNT, and generally lower σ_{peak} (Fig. 2D).

However, similar to $IPN-Lin_{100}UPy_{7.5}FMA_{7.5}$, $BCN-Blk_{100}UPy_{3.75}FMA_{3.75}-1\%CNT$ containing equimolar DA-UPy cross-links resulted in a σ_{peak} of 5.9 ± 0.04 MPa compared to $IPN-Lin_{100}UPy_{7.5}FMA_{7.5}1\%CNT$ with σ_{peak} of 3.2 ± 0.2 MPa. Hence tri-block $BCN-Blk_{100}UPy_{3.75}FMA_{3.75}$ leads to not only higher self-healing efficiency (Fig. 2E), but also higher mechanical performance (Fig. 2E) compared to $IPN-Lin_{100}UPy_{7.5}FMA_{7.5}$ (Fig. 2A). This suggests that at high strains, the block like structure, with domains of dense UPy and DA crosslinks leads to higher tolerance to stress, while enabling CNT reinforcement and load transfer.

A second control material was designed using GMA instead of FMA as a cross-linking motif leading to $BCN-Blk_{100}UPy_{3.75}GMA_{3.75}$. Fig. 2F reveals that addition of 1 wt% CNT to $BCN-Blk_{100}UPy_{3.75}GMA_{3.75}$ made no significant impact on material properties (healing, ε_{break}, and σ_{peak}) of $BCN-Blk_{100}UPy_{3.75}GMA_{3.75}1\%CNT$ compared to $BCN-Blk_{100}UPy_{3.75}GMA_{3.75}0\%CNT$. This indicates that poor
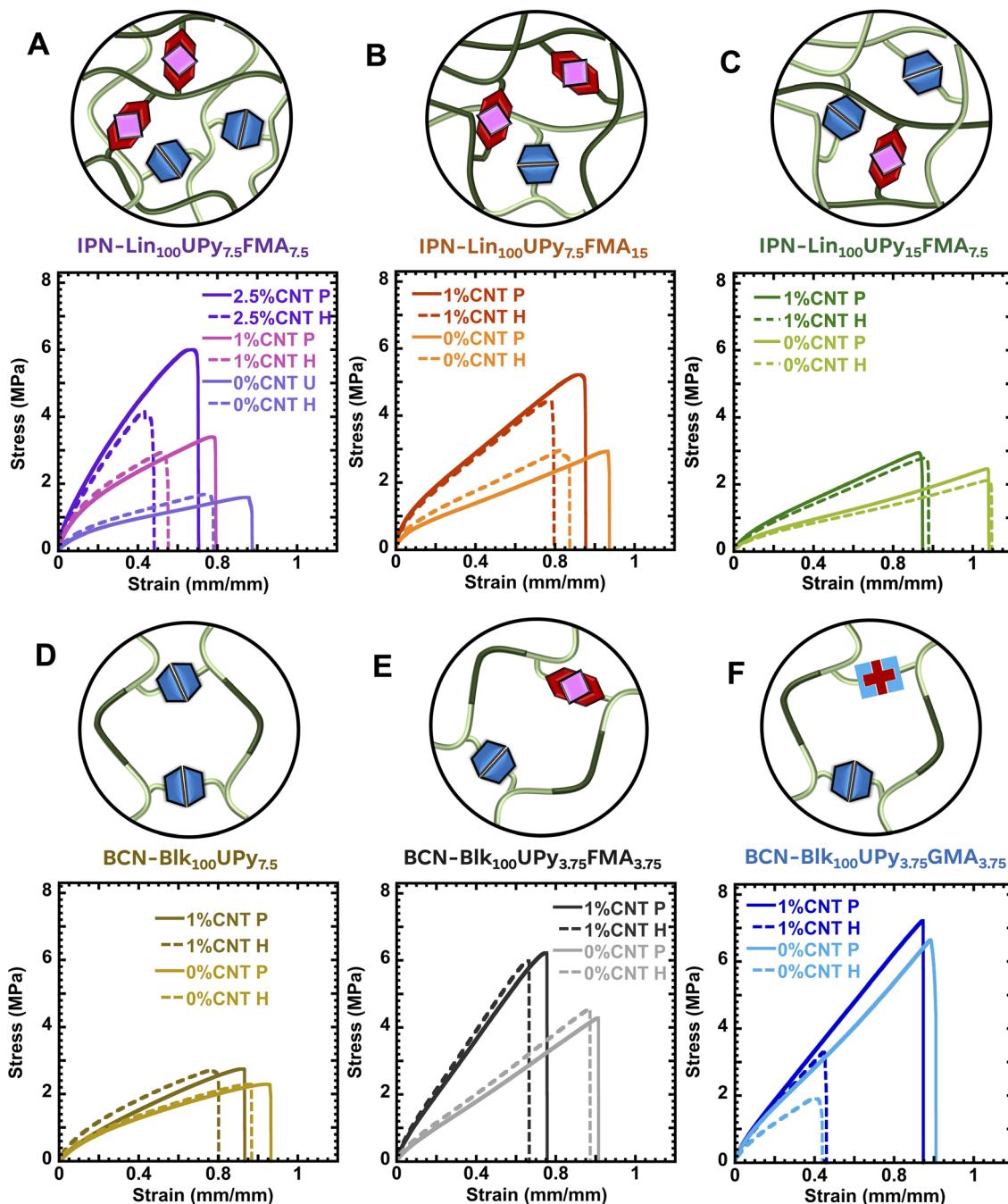
Fig. 2 Architectural features and mechanical properties of reinforced and unreinforced (A) IPN-Lin$_{100}$UPy$_{7.5}$FMA$_{7.5}$, (B) IPN-Lin$_{100}$UPy$_{7.5}$FMA$_{15}$, (C) IPN-Lin$_{100}$UPy$_{15}$FMA$_{7.5}$, (D) BCN-Blk$_{100}$UPy$_{7.5}$, (E) BCN-Blk$_{100}$UPy$_{3.75}$FMA$_{3.75}$, and (F) BCN-Blk$_{100}$UPy$_{3.75}$GMA$_{3.75}$. P represents a pristine sample and H represents a thermally healed sample.

healing and poor mechanical enhancement observed is due to weak interaction between the polymer chains and CNT nanofillers. Since the epoxy group on GMA of BCN-Blk$_{100}$UPy$_{3.75}$GMA$_{3.75}$ lacks the ability to chemically bond polymer chains to CNT nanofillers, poor nanoreinforcement performance is observed. The poor dynamic performance (*i.e.*, self-healing) observed is due to the non dynamic nature of GMA cross-linked with diamines (Scheme S3†) with all

dynamic exchange coming from UPy units as observed in Fig. 3B. To further confirm this, BCN-Blk$_{100}$UPy$_{7.5}$ which is also a control material, gave >1 order magnitude higher healing efficiency compared to BCN-Blk$_{100}$UPy$_{3.75}$GMA$_{3.75}$. Overall, the very poor reinforcement in control materials that do not contain FMA units, specifically BCN-Blk$_{100}$UPy$_{3.75}$GMA$_{3.75}$ and BCN-Blk$_{100}$UPy$_{7.5}$, indicate that efficient load transfer from the matrix to the CNT reinforce-

© 2023 The Author(s). Published by the Royal Society of Chemistry

RSC Appl. Polym., 2023, **1**, 30–45 | **37**
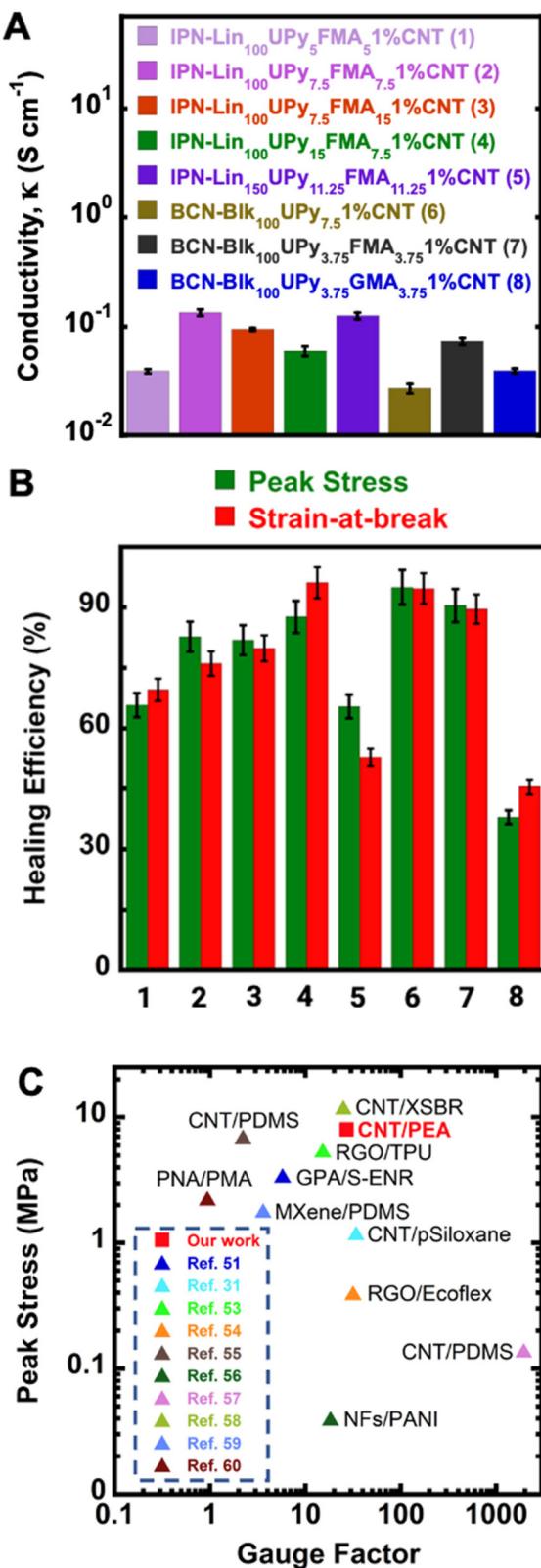
Fig. 3 (A) Electrical conductivity of all 1 wt% CNT reinforced DPNs in this study. DPN designations (1–8) are used in (B). (B) Healing efficiency determined by the recovery of breaking (tensile) stress as well as breaking strain. (C) Ashby plot of σ_{peak} and GF of IPN-Lin$_{100}$UPy$_{7.5}$FMA$_{7.5}$2.5% CNT compared to other reported conductive polymer composites in literature.[33,54,56–63]

ment requires the furan units to bond to the CNT surface in these materials. This highlights the potential of the direct and mild modification of CNT surfaces using Diels–Alder chemistry from furan.

The surface morphology of IPN-Lin$_{100}$UPy$_{7.5}$FMA$_{7.5}$2.5% CNT and IPN-Lin$_{100}$UPy$_{7.5}$FMA$_{7.5}$0%CNT was analyzed using scanning electron microscopy as represented in Fig. S5.† No distinctive feature was observed in the micrographs of unreinforced IPN-Lin$_{100}$UPy$_{7.5}$FMA$_{7.5}$0%CNT. However, reinforced IPN-Lin$_{100}$UPy$_{7.5}$FMA$_{7.5}$2.5%CNT revealed distinct features both on the surface and cross-sectional micrographs that suggests the presence of a nanofiller as shown in Fig. S5(C and D).† The presence of two types of dynamic bonds contributed to the healing efficiency observed in all CNT reinforced DPNs represented in Fig. 3B. One is dynamic H-bond between polymer chains *via* UPy motifs which reversibly associate and dissociate under temperate room conditions, providing an attractive force for better damage repair and healability.[35] The other is the dynamic covalent DA bonds between polymer chains *via* FMA furan groups and BMI cross-linker which was can reversibly dissociate and associate at elevated temperatures.[31] Generally, IPN-based IPN-Lin$_{100}$UPy$_{15}$FMA$_{7.5}$ and BCN-based BCN-Blk$_{100}$UPy$_{7.5}$ had the highest healing efficiencies and this most likely due to their possession of abundant UPy driven quadrupole H-bonding, which contributes significantly to healing properties.[54,55] In particular, the generation of domains of high DA and UPy crosslink density appears to facilitate self-healing, consistent with prior studies on blocky multiply dynamic networks.[40]

Electrical properties and applications of DPNs

Electrical conductivity. Composites of elastomers such as polyurethane, natural rubber, polydimethylsiloxane, as well as poly(styrene-*b*-butadiene-*b*-styrene) have been employed as electrically conducting materials.[64,65] Yet, most of these elastomers exhibit poor healing properties after fracture, hence decreasing their useful lifetime. Additionally, research has shown that CNTs have better interaction with soft matrices than brittle ones,[47] hence utilizing polyEA/CNT in this work is advantageous since PolyEA often have T_g that is below room temperature.[49,50] Advances in healable flexible electronics and robotics has attracted substantial attention and is currently in high demand.[21,22] Therefore, we investigated the electrical conductivity (κ) of DPNs.

Fig. 3A gives the conductivity (κ) for all 1 wt% CNT reinforced DPNs. The highest κ values were observed in IPN-Lin$_{100}$UPy$_{7.5}$FMA$_{7.5}$1%CNT and the longer-chain variant IPN-Lin$_{150}$UPy$_{11.25}$FMA$_{11.25}$1%CNT with 0.099 ± 0.003 and 0.125 ± 0.007 S cm^{-1} respectively. IPN-Lin$_{100}$UPy$_{7.5}$FMA$_{7.5}$2.5%CNT with higher CNT loading gave a κ of 0.402 ± 0.005 S cm^{-1} which is higher than that of the 1 wt% CNT variant by over a factor of 4, thus confirming the contribution of CNT nanofiller to conductive properties of reinforced DPNs. Based on the conductivity profile of all DPNs reported in Fig. 3A, it is evident that equimolar DA and UPy cross-linked IPN-Lin$_{100}$UPy$_{7.5}$FMA$_{7.5}$ and the longer chain length variant IPN-Lin$_{150}$UPy$_{11.25}$FMA$_{11.25}$ had better κ

values overall. This again confirms the better performance of IPN-Lin$_{100}$UPy$_{7.5}$FMA$_{7.5}$ material both mechanically and electrically which suggests they have better compatibility with CNT nanofillers. Although BCN-Blk$_{100}$UPy$_{3.75}$FMA$_{3.75}$1%CNT exhibited a competitive mechanical performance, IPN-Lin$_{100}$UPy$_{7.5}$FMA$_{7.5}$1%CNT possessed better electrical conductivity (Fig. 3A), hence making IPN-Lin$_{100}$UPy$_{7.5}$FMA$_{7.5}$ an all-around better material for further studies.

Given the electrical conductivity of DPNs in this study, a key parameter to be considered is the gauge factor (GF) which is defined as the ratio of fractional changes in electrical resistance, R, to the ratio of fractional change in material length (i.e., strain):[66]

$$\text{GF} = (\Delta R/R)/(\Delta L/L) = (\Delta R/R)/\varepsilon \qquad (1)$$

For perspective, the GF of metallic foils under deformation are typically 2–5 mostly owing to changes in the cross-sectional area and length of the metal instead of changes in resistivity as response to mechanical deformation.[67] Elastomeric semiconducting materials however have better strain gauging for precision measurements because they can withstand severe bending (flexion) or stretching due to the presence of polymeric substrates.[68,69] Hence to further investigate the electrical properties of DPNs, the relative change in resistance denoted by $\frac{[R/R_0]}{\varepsilon}$ at only 60% strain was calculated and a GF of 27 ± 3 was obtained for IPN-Lin$_{100}$UPy$_{7.5}$FMA$_{7.5}$2.5%CNT. The GF value is often used to evaluate the sensitivity of a strain sensor where R, R_0, ε represent the testing resistance, initial resistance, and applied strain respectively. Fig. 3C gives the comparison of IPN-Lin$_{100}$UPy$_{7.5}$FMA$_{7.5}$2.5%CNT GF value relative to some previously reported electrically conductive self-healing polymer nanocomposites. Additionally, comparison of σ_{peak} gives insight into the mechanical performance of our IPN-Lin$_{100}$UPy$_{7.5}$FMA$_{7.5}$2.5%CNT material.
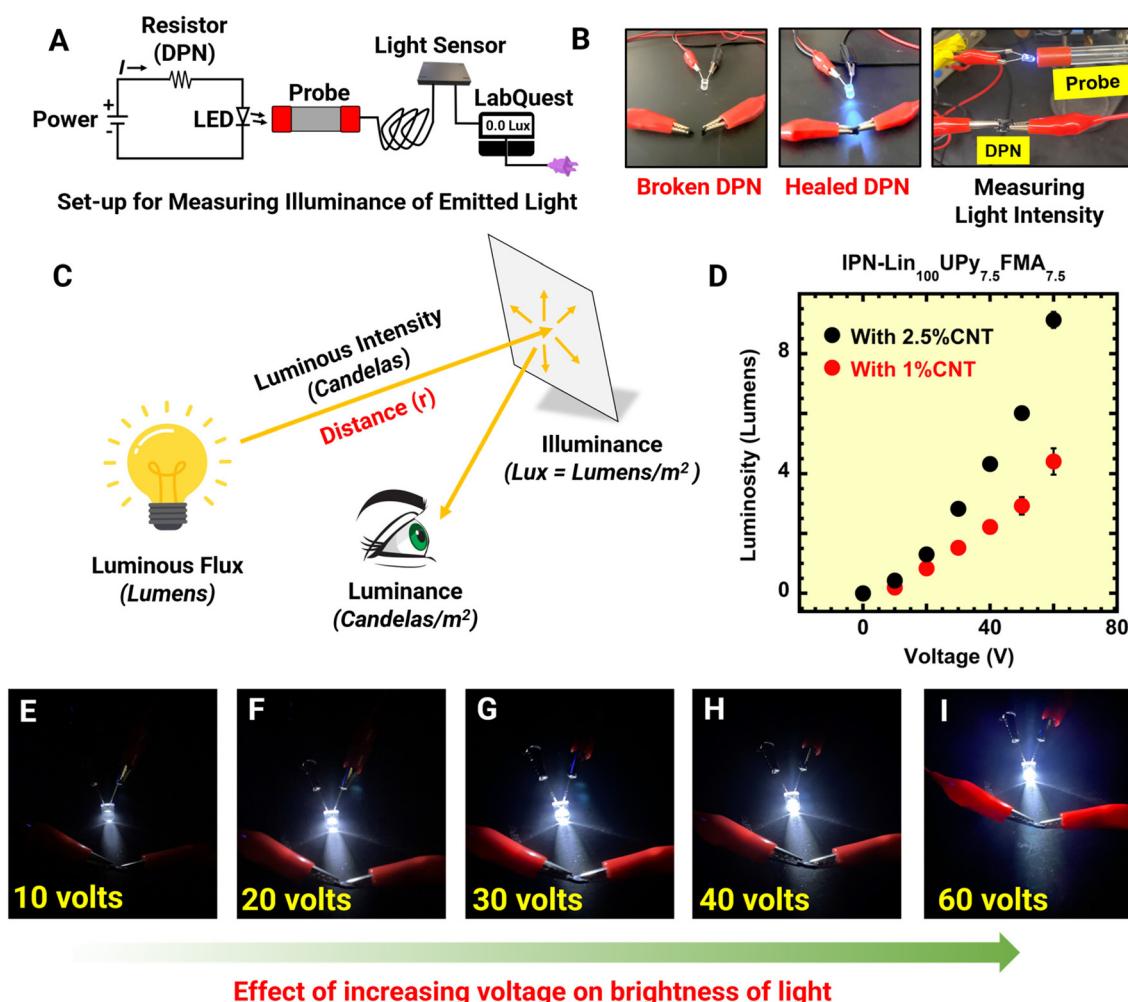

Fig. 4 Light intensity measurements of IPN-Lin$_{100}$UPy$_{7.5}$FMA$_{7.5}$ materials. (A) Set-up for measuring the illuminance of light in lux. (B) Impact of fracture and repair of DPN on LED in a circuit system. (C) Luminosity illustration. (D) Impact of increasing PD on luminosity of diode connected to IPN-Lin$_{100}$UPy$_{7.5}$FMA$_{7.5}$2.5%CNT and IPN-Lin$_{100}$UPy$_{7.5}$FMA$_{7.5}$1%CNT employed as electrical resistors, (E–I) Effect of increasing PD on the brightness of LED.

Application of DPNs as materials for controlled current flow and LED lighting. A simple electrical circuit was created with IPN-Lin$_{100}$UPy$_{7.5}$FMA$_{7.5}$2.5%CNT employed as a resistor and a dimmable light emitting diode (LED) was used to confirm the flow of current (Fig. 4B). The circuit can be broken by damaging the DPN resistor using a razor blade and when repaired under thermal stimulus, the flow of current resumes and the LED lights up as shown in Fig. 4B. A light sensor equipped with a sensing probe and LabQuest was used to determine the LED brightness in response to current applied across the circuit as illustrated in Fig. 4A. The intensity of emitted light was measured by placing the sensing probe at a fixed position relative to the LED connected to the circuit. The concept of measuring luminous intensity that did not depend on the properties of a particular lamp was first proposed in 1881.[70] Luminous flux is the total amount of light a source emits, consolidated over the entire angular span of measured light and the unit is in lumens. Luminous intensity is defined as the measure of light that shines in a given direction from the source. While the amount of light that shines on a surface is referred to as illuminance, measured in lumens m^{-2} or lux. The relationship of these photometric terminologies has been illustrated in Fig. 4C.

IPN-Lin$_{100}$UPy$_{7.5}$FMA$_{7.5}$2.5%CNT and IPN-Lin$_{100}$UPy$_{7.5}$FMA$_{7.5}$1%CNT were used as soft electronic materials for regulating the amount of current flowing through a circuit and consequently the luminous intensity of LED connected to the circuit (Fig. 3D and 4). Increasing the source potential difference (PD) of the circuit system from 10, 20, 30, 40, 50, and 60 V directly results in a progressive rise in luminosity as demonstrated in Fig. 4B. Although IPN-Lin$_{100}$UPy$_{7.5}$FMA$_{7.5}$2.5%CNT and IPN-Lin$_{100}$UPy$_{7.5}$FMA$_{7.5}$1%CNT showed similar trends, IPN-Lin$_{100}$UPy$_{7.5}$FMA$_{7.5}$2.5%CNT had a steeper rise in luminosity due to the higher CNT loading facilitating electrical percolation and current flow through the material compared to IPN-Lin$_{100}$UPy$_{7.5}$FMA$_{7.5}$1%CNT. Furthermore, Fig. 4(C–G) shows a continuous increase in illuminance/brightness of LED as PD applied to the circuit system increases. This highlights the potential of CNT reinforced IPN-Lin$_{100}$UPy$_{7.5}$FMA$_{7.5}$ for next generation electronic materials for smart lighting devices where light intensity could be regulated *via* integrated conductive elastomeric materials that controls the current.

Application of DPNs as custom resistors and strain sensor. Organic resistors with on-demand customization are one of the most competitive options for novel solutions to data storage in flexible electronics.[71] Custom resistors in this work were enabled by self-healing of IPN-Lin$_{100}$UPy$_{7.5}$FMA$_{7.5}$2.5% CNT [denoted *L* for low resistance] and IPN-Lin$_{100}$UPy$_{7.5}$FMA$_{7.5}$1%CNT [denoted H for high resistance] with different CNT loadings as illustrated in Fig. 5A to obtain 4 resistors. The custom resistors are denoted by the proportion of L and H, with 70%H–30%L denoting a resistor comprised of 70% of the high resistance IPN-Lin$_{100}$UPy$_{7.5}$FMA$_{7.5}$1%CNT and 30% of the low resistance IPN-Lin$_{100}$UPy$_{7.5}$FMA$_{7.5}$2.5% CNT (Table 2). Healing was achieved after heating at 90 °C for
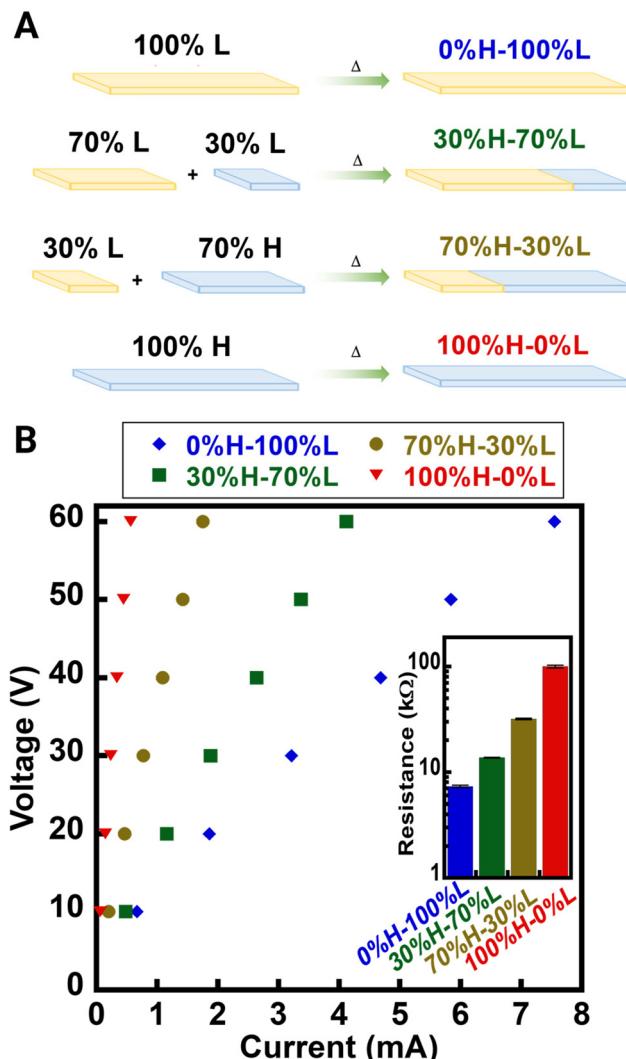
Fig. 5 (A) Illustration of how custom resistors are achieved *via* healing using IPN-Lin$_{100}$UPy$_{7.5}$FMA$_{7.5}$2.5%CNT and IPN-Lin$_{100}$UPy$_{7.5}$FMA$_{7.5}$1% CNT, (B) Impact of current on custom resistors using current–voltage plots, and the measured resistance (inset) of each resistor.

16 hours. CNT reinforced IPN-Lin$_{100}$UPy$_{7.5}$FMA$_{7.5}$ materials were used as resistors in the circuit set-up shown in Fig. S6† and current flow across the circuit was measured. It was found that all four DPNs acted as resistors with the ability to allow a certain amount of electrical current through the circuit. Fig. 5B shows the amount of current that flows a circuit when each resistor is used and the trend that emanates in response to increased potential difference. IPN-Lin$_{100}$UPy$_{7.5}$FMA$_{7.5}$2.5% CNT with electrical conductivity 0.402 ± 0.005 S cm^{-1} designated as 0%H–100%L permitted more electricity flow into the circuit compared to IPN-Lin$_{100}$UPy$_{7.5}$FMA$_{7.5}$1%CNT with an electrical conductivity of 0.099 ± 0.003 S cm^{-1} designated as 100%H–0%L.

Through self-healing ability in both materials, 70%H–30%L and 30%H–70%L were achieved with electrical conductivity that falls in-between 100%H–0%L and 0%H–100%L hence

Table 2 Custom resistors achieved *via* thermal healing of IPN-Lin$_{100}$UPy$_{7.5}$FMA$_{7.5}$2.5%CNT and IPN-Lin$_{100}$UPy$_{7.5}$FMA$_{7.5}$1%CNT

Designation for custom resistors	DPN combinations	Resistance [kΩ]
0%H–100%L	100% of IPN-Lin$_{100}$UPy$_{7.5}$FMA$_{7.5}$2.5%CNT	7.3 ± 0.2
30%H–70%L	(70% of IPN-Lin$_{100}$UPy$_{7.5}$FMA$_{7.5}$2.5%CNT) + (30% of IPN-Lin$_{100}$UPy$_{7.5}$FMA$_{7.5}$1%CNT)	13.7 ± 0.1
70%H–30%L	(30% of IPN-Lin$_{100}$UPy$_{7.5}$FMA$_{7.5}$2.5%CNT) + (70% of IPN-Lin$_{100}$UPy$_{7.5}$FMA$_{7.5}$1%CNT)	31.9 ± 0.6
100%H–0%L	100% IPN-Lin$_{100}$UPy$_{7.5}$FMA$_{7.5}$1%CNT	100 ± 3

facilitating the modulation of electrical properties besides through changing CNT loadings (Table 2). Movies 1–3 shows the function of IPN-Lin$_{100}$UPy$_{7.5}$FMA$_{7.5}$2.5%CNT as a resistor in a circuit wherein absence of DPN causes an overflow of current towards the LED which consequently damages the diode whereas addition of DPN resistor regulates the amount of current that flows to the LED. We observed that after using a 9 V battery, only a PD of 2.6 V was measured across the LED suggesting that the PD across the IPN-Lin$_{100}$UPy$_{7.5}$FMA$_{7.5}$2.5% CNT was ~6.4 V. Further investigation confirms that increasing CNT loadings decreases the electrical resistance in IPN-Lin$_{100}$UPy$_{7.5}$FMA$_{7.5}$ materials (Fig. S7†).

To gain insight into the impact of prolonged exposure to electrical current, IPN-Lin$_{100}$UPy$_{7.5}$FMA$_{7.5}$2.5%CNT was integrated into a circuit system with a 9 V battery leading to illumination of LED in the circuit as shown in Fig. S8.† The system was left untampered for 12 days after which the battery voltage was depleted to <1 V (measured using a multimeter). However, when the depleted battery is replaced with a new 9 V battery, the LED bulb produces light and IPN-Lin$_{100}$UPy$_{7.5}$FMA$_{7.5}$2.5% CNT still acts as a resistor by limiting the flow of current towards the LED. This indicates that IPN-Lin$_{100}$UPy$_{7.5}$FMA$_{7.5}$2.5%CNT and LED were not affected by prolonged use in electronic applications, and suitable for long term electrical applications. To confirm the ability of IPN-Lin$_{100}$UPy$_{7.5}$FMA$_{7.5}$ to act as resistors, a series of measurements were collected (Table S4†) enabled by circuit systems illustrated in Fig. S9.† IPN-Lin$_{100}$UPy$_{7.5}$FMA$_{7.5}$2.5%CNT consistently restricted the current flow from a PD of 10, 20, 30, 40, 50, and 60 V ensuring that only the necessary PD across the diode remained at the ~2.5 V needed to power the LED, hence preventing it from damage.

Additionally, the detection of bending and unbending (flexion) motions of IPN-Lin$_{100}$UPy$_{7.5}$FMA$_{7.5}$2.5%CNT was achieved, indicating piezoresistive behavior.[33] Fig. 6 shows changes in the relative current flowing through IPN-Lin$_{100}$UPy$_{7.5}$FMA$_{7.5}$2.5%CNT in response to multiple bending and unbending cycles, confirming the ability of the material to convert mechanical deformation into electrical signals, highlighting the potential for strain sensing functions for IPN-Lin$_{100}$UPy$_{7.5}$FMA$_{7.5}$2.5%CNT. This is consistent with the excellent gauge factor performance in Fig. 3C. Sensitivity of IPN-Lin$_{100}$UPy$_{7.5}$FMA$_{7.5}$2.5%CNT was further confirmed in a simple demonstration using a multimeter (Fig. S10†) which shows an increase in resistance under bending and decreased resistance when the material was straightened. This indicates that there is less resistance to the flow of current across IPN-Lin$_{100}$UPy$_{7.5}$FMA$_{7.5}$2.5%CNT under little or no mechanical deformation, consistent with other electrically conductive polymer nanocomposites.[33,72]
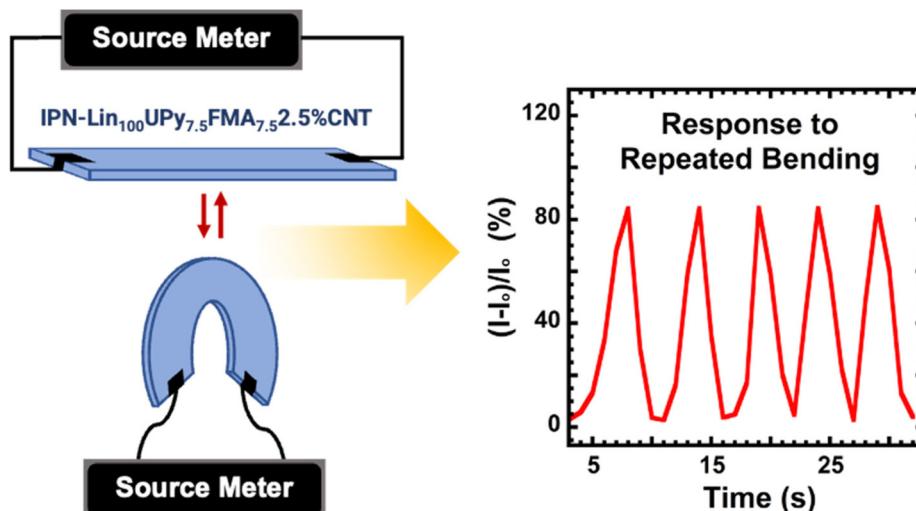
Fig. 6 Illustration of IPN-Lin$_{100}$UPy$_{7.5}$FMA$_{7.5}$2.5%CNT material bending in connection to a source meter depicting potential to function as a strain sensor.

© 2023 The Author(s). Published by the Royal Society of Chemistry

RSC Appl. Polym., 2023, **1**, 30–45 | **41**

Conclusion

In summary, we present the facile synthesis of a new class of self-healable dynamic polymer nanocomposites (DPNs). The multifunctionality of the DPNs was demonstrated through applications in responsive lighting systems, customizable resistors, and their potential as strain sensing composite materials. Combining dynamic covalent Diels–Alder (DA) chemistry of FMA pendant furan groups with BMI cross-linkers and dynamic quadruple H-bonding of UPy cross-linking units afforded multiple DPN materials with distinct architectural designs. FMA enabled a mild *in situ* [4 + 2] DA reaction with π-bonds on the CNT surface, resulting in effective transfer of load/stress from polymer chains to CNT nanofillers without pre-functionalization. Well-designed interpenetrated (IPN) and block (BCN)-based DPNs were synthesized, each with different architectural features. Structure–property studies revealed that polymer architecture not only impacts mechanical performance but also the electrical properties of DPNs. IPN-Lin$_{100}$UPy$_{7.5}$FMA$_{7.5}$ materials generally outperform other IPN and BCN-based DPN materials in this work. IPN-Lin$_{100}$UPy$_{7.5}$FMA$_{7.5}$ materials had better mechanical enhancement upon addition of CNT nanofillers and higher electrical conductivity of CNT reinforced IPN-Lin$_{100}$UPy$_{7.5}$FMA$_{7.5}$ materials, resulting in a gauge factor of 27 ± 3. This goes to show that equimolar use of Diels–Alder (DA) and UPy H-bonding cross-link units in IPN systems in combination with macromolecular engineered interaction with CNT nanofillers favored the thermo-mechanical, electrical, and dynamic properties of resulting in multifunctional DPN materials. The results suggest that using equal mole% equivalents of DA and UPy cross-links is an effective strategy for designing DPNs with CNT nanofillers compared to unequal distribution of DA and UPy cross-linking motifs. In addition to demonstrated application of IPN-Lin$_{100}$UPy$_{7.5}$FMA$_{7.5}$2.5%CNT and IPN-Lin$_{100}$UPy$_{7.5}$FMA$_{7.5}$1% CNT as electronic materials for regulating smart dimmable LED lighting systems, DPNs in this work also exhibited remarkable self-healing traits which enabled their application as customizable resistors. Electrical and mechanical properties combined with unique network structures of DPNs led to overall multifunctional applications including strain sensing. DPNs introduced in this work could lend themselves to other promising applications in multifunctional flexible electronics such as human vocalization, acoustic vibration, human motion detection, and portable smart lighting systems.

Experimental section

Materials and reagents

All starting materials, reagents, and solvents were purchased from commercial sources and used directly without further purification unless specified otherwise. 2-(((6-(3-(6-Methyl-4-oxo-1,4-dihydropyrimidin-2-yl)ureido)hexyl)carbamoyl)-oxy) ethyl acrylate (UPy) and (2-propionic acid)yldodecyl trithiocarbonate (PADTC) were synthesized as outlined in literature.[73]

Synthesis of a typical IPN-based DPN using poly[EA$_{100}$-Upy$_{7.5}$-FMA$_{3.75}$]

Synthesis of FMA network (poly[EA$_{100}$-FMA$_{7.5}$]). To a 50 mL round bottom flask equipped with a magnetic stir bar, azobisisobutyronitrile (AIBN) [0.016 g, 0.099 mmol], PADTC [0.175 g, 0.499 mmol], furfuryl-methacrylate (FMA) [0.622 g, 3.75 mmol], Ethyl acrylate (EA) [5.00 g, 49.9 mmol], and Toluene solvent [8.72 g] were added. The reaction mixture was sealed and deoxygenated under nitrogen gas for 15 minutes. The deoxygenated mixture was transferred to an oil bath and stirred at 65 °C for 8 hours. Resulting poly(EA$_{100}$-FMA$_{7.5}$) was confirmed by ^{1}H-NMR indicating 78% conversion and SEC gave a dispersity Đ of 1.31. The polymer was recovered after precipitating in hexanes and dried in a vacuum oven overnight using a weighed-out Erlenmeyer flask to remove excess solvent. After drying, 5.2 g experimental weight of the polymer was obtained and recorded.

Synthesis of UPy network (poly[EA$_{100}$-UPy$_{7.5}$]). To a 50 mL round bottom flask equipped with a magnetic stir bar, AIBN [0.016 g, 0.099 mmol], PADTC [0.175 g, 0.499 mmol], UPy [1.54 g, 3.75 mmol], EA [5.00 g, 49.9 mmol], and DMF solvent [10 g] were added. The reaction mixture was sealed and deoxygenated under nitrogen gas for 15 minutes. The deoxygenated mixture was transferred to an oil bath and stirred at 65 °C for 24 hours leading to poly[EA$_{100}$-UPy$_{7.5}$] which was confirmed by ^{1}H-NMR, indicating >95% conversion. SEC gave a dispersity Đ of 1.17 and the polymer was not precipitated due to high conversion.

CNT reinforcement and IPN formation through post polymerization dynamic H-bonding and Diels–Alder cross-linking. FMA and UPy networks were combined by transferring 5.2 g of unprecipitated (poly[EA$_{100}$-UPy$_{7.5}$] in DMF) into 5.2 g of precipitated poly[EA$_{100}$-FMA$_{7.5}$]. The resulting IPN was subjected to ultrasonication for 30 minutes to obtain a homogenous mixture of poly[EA$_{100}$-FMA$_{7.5}$] and poly[EA$_{100}$-UPy$_{7.5}$] in DMF. Dynamic covalent cross-linking was obtained by addition of $\frac{1}{2}$ mole equivalent of 1,1′-(methylene-di-4,1-phenylene)bismaleimide (BMI) with respect to the mole of FMA present and sonicated for 30 min. This was followed by addition of 0, 1, or 2.5 weight percent amount of CNT to the reaction flask with respect to overall IPN polymer weight. The IPN and CNT mixture were allowed to sonicate for 60 minutes to give even dispersion of CNT in the polymer matrix. The reaction contents were then transferred into a dog-bone shaped Teflon mold and covered with glass for 16 hours at 50 °C leading to dynamic covalent cross-linking *via* Diels–Alder reaction of FMA motifs and H-bonding between UPy motifs. Once cross-linked and molded, the dog bone shaped materials were removed from the Teflon mold and allowed to dry in a fume hood for 2 days and overnight in a vacuum oven. The same procedure was followed for longer chain length poly[EA$_{150}$-Upy$_{11.25}$-FMA$_{11.25}$], less cross-linked poly[EA$_{100}$-Upy$_5$-FMA$_5$], double FMA equivalent poly[EA$_{100}$-Upy$_{7.5}$-FMA$_{15}$], and double UPy equivalent poly[EA$_{100}$-Upy$_{15}$-FMA$_{7.5}$]. The composition and SEC data of all IPN polymers are reported in Fig. S1 and Table S1.†

Synthesis of BCN-based DPN using poly[EA$_{20}$-UPy$_{3.75}$]-*b*-[EA$_{60}$]-*b*-[EA$_{20}$-FMA$_{3.75}$]

To a 50 mL round bottom flask equipped with magnetic stir bar, AIBN, (0.008 g, 0.045 mmol), PADTC [0.159 g, 0.45 mmol], UPy [0.7 g, 1.7 mmol], EA [0.91 g, 9.1 mmol] and 3.55 g of DMF were added. The reaction mixture was sealed and deoxygenate for 15 minutes. After which the reaction mixture was stirred at 65 °C for 24 h. The resulting poly[EA$_{20}$-UPy$_{3.75}$] polymer was confirmed by ^{1}H-NMR indicating >95% conversion. To carry out the chain extension, AIBN [0.008 g, 0.045 mmol], EA [2.73 g, 27.3 mmol] and 2.80 g of DMF were added to the above reaction mixture. The reaction mixture was sealed and deoxygenate for 15 minutes. The AB block chain extension reaction was then carried out at 65 °C for 24 hours with continuous stirring. Monomer conversion of AB poly[EA$_{20}$-UPy$_{3.75}$]-*b*-[EA$_{60}$] was confirmed to be >95% using ^{1}H-NMR. For the final chain extension to obtain ABC-type polymer, AIBN [0.0080 g, 0.045 mmol], FMA [0.28 g, 1.7 mmol], EA [0.91 g, 9.1 mmol] and 3.10 g of DMF was added to the reaction mixture and deoxygenated for 15 minutes. The reaction was then carried out at 65 °C for 10 hours with continuous stirring. After 24 h, monomer conversion (78%) of poly[EA$_{20}$-UPy$_{3.75}$]-*b*-[EA$_{60}$]-*b*-[EA$_{20}$-FMA$_{3.75}$] was confirmed using ^{1}H-NMR. The compositions and SEC characterization data of all the BCN polymers are reported in Fig. S2 and Table S1.†

Self-healing experiment

Materials subjected to self-healing were first sliced in half using a razor blade and the two separate ends of such material are then pressed back together at the sliced area using mild pressure from fingers. Afterwards all materials, both pristine (P) and healable (H) were placed in an oven at 90 °C for 24 hours to expose the materials to equivalent thermal conditions. Samples were then subjected to tensile tests. For the time evolution self-healing test, similar steps were followed except the materials were heated for 1, 7, 14, and 24 hours at 90 °C respectively as reported in Fig. S3(D and E).†

Electrical conductivity [κ]

Resistance (R) was measured using a Keithley 2450 Source Measure Unit Instrument. The ohmmeter setting was used to determine specimen resistance. A 4-point probe system was used for all CNT reinforced samples. The resistivity [ρ] was obtained by dividing resistance R by the length [l] of materials and multiplying by cross-sectional area A.

$$\rho = \frac{RA}{l} \tag{2}$$

Electrical conductivity [κ] was determined using the inverse of resistivity.

$$\kappa = \rho^{-1} \tag{3}$$

Illumination measurement

A probe for light sensing was connected to a lab quest which was connected to a power source. The light probe was positioned at an approximate distance of 2.5 mm from a lighted diode con-nected to an electrical circuit where a DPN was employed as an organic resistor. Illumination in lux was obtained from the lab quest and used to determine luminosity in lumens while changing the potential difference (PD) applied to the circuit from 10, 20, 30, 40, 50, and 60 V. Luminosity [Φ] was determined by multiplying illumination [E] and surface area of the spherical diode [A] leading to a plot of Φ against voltage showing the impact of increasing PD on Φ and potential of DPNs as organic resistors in electrical circuits as demonstrated in Fig. 4.

$$\text{Illumination } E(\text{lux}) = \frac{[\text{Luminous flux or luminosity } \Phi(\text{lumen})]}{[\text{Surface area of a sphere}(4\pi r)^2)]} \tag{4}$$

Custom resistor test

Experiment was carried out by setting-up a circuit and measuring the amount of current [I] traveling from an organic resistor to the diode. Impact of changing the PD applied to the circuit on the current is recorded for each resistor and added to a joint plot showing the result of customizing or tuning the properties of organic resistors.

Strain sensing

IPN-Lin$_{100}$UPy$_{7.5}$FMA$_{7.5}$2.5%CNT was connected to a Keithley 2450 Source Meter which was set to Ammeter mode to measure current. A 2-point probe system was used to link the DPN to the meter for ease of bending. Repeated bending of IPN-Lin$_{100}$UPy$_{7.5}$FMA$_{7.5}$2.5%CNT at a combined 180° gave fluctuating wave response in current measurement over time. A plot of $\Delta I/I_0$ (%) on the y-axis against Time (s) on the x-axis shows response of the material to repeated bending in Fig. 6.

Young's modulus [Y] calculation

Incompressible Ogden hyper-elastic constitutive law similar to previous reports in our group[31,35,55] (eqn (5)) was used to model the tensile response of materials.

$$\sigma_{\text{eng}} = \frac{2G}{\alpha}\left[\lambda^{\alpha-1} - \lambda^{-1-\left(\frac{\alpha}{2}\right)}\right] \tag{5}$$

σ_{eng} is the engineering stress. α is the strain hardening exponent. G is the shear modulus, and λ is the stretch ratio. G and α were found for each sample by fitting eqn (5) to the experimental mechanical data. Eventually, elastic modulus [Y] was found from eqn (6) assuming an incompressible solid [$\nu = 0.5$].

$$Y = 2G[1 + \nu] \tag{6}$$

Strain calculation

Strain was evaluated from eqn (7).

$$\varepsilon = \left[\frac{L - L_0}{L_0}\right] \tag{7}$$

where L is the length of the elongated sample and L_0 is the initial length of the specimen.

$\varepsilon_{\text{break}}$ is the strain at break.

© 2023 The Author(s). Published by the Royal Society of Chemistry

RSC Appl. Polym., 2023, **1**, 30–45 | **43**

Stress calculation

Stress was evaluated from eqn (8).

$$\sigma = \frac{F}{A} \tag{8}$$

where F represents uniaxial force and A is the cross-sectional area of the material experiencing the applied force. This work focuses on the engineering stress which was calculated from the original area of the sample prior to force application.

Author contributions

O. J. D. and D. K. conceptualized the materials studied with D. K. O. J. D and C. J. T. involved in conceptualization of applications. O. J. D., I. O. R., I. J. A., C. P. M., L. P., K. W., and D. D. synthesized the materials and characterized the structures. O. J. D. and D. K. analyzed the results. O. J. D. prepared the manuscript, D. K. contributed to manuscript development. All authors reviewed and edited the manuscript.

Conflicts of interest

The authors declare no conflict of interest.

Acknowledgements

References

1 B. C. K. Tee, C. Wang, R. Allen and Z. Bao, *Nat. Nanotechnol.*, 2012, **7**, 825–832.

2 R. F. Shepherd, A. A. Stokes, R. M. D. Nunes and G. M. Whitesides, *Adv. Mater.*, 2013, **25**, 6709–6713.

3 Y. Xin, Y. Lou, H. Liu, D. Wu and J. Zhang, *Adv. Mater. Technol.*, 2021, **6**, 1–9.

4 S. Park, G. Thangavel, K. Parida, S. Li and P. S. Lee, *Adv. Mater.*, 2019, **31**, 1805536.

5 Z. Wang, Y. Liu, D. Zhang, K. Zhang, C. Gao and Y. Wu, *Compos. Sci. Technol.*, 2021, **216**, 109042.

6 D. Chen, D. Wang, Y. Yang, Q. Huang, S. Zhu and Z. Zheng, *Adv. Energy Mater.*, 2017, 7.

7 C. J. Thrasher, Z. J. Farrell, N. J. Morris, C. L. Willey and C. E. Tabor, *Adv. Mater.*, 2019, **31**, 1903864.

8 E. F. Gomez, S. V. Wanasinghe, A. E. Flynn, O. J. Dodo, J. L. Sparks, L. A. Baldwin, C. E. Tabor, M. F. Durstock, D. Konkolewicz and C. J. Thrasher, *ACS Appl. Mater. Interfaces*, 2021, **13**, 28870–28877.

9 K. Myny, *Nat. Electron.*, 2018, **1**, 30–39.

10 A. M. Hussain and M. M. Hussain, *Adv. Mater.*, 2016, **28**, 4219–4249.

11 S. K. Arya, C. C. Wong, Y. J. Jeon, T. Bansal and M. K. Park, *Chem. Rev.*, 2015, **115**, 5116–5158.

12 Y. Cheng, R. Wang, J. Sun and L. Gao, *Adv. Mater.*, 2015, **27**, 7365–7371.

13 P. Lavrador, M. R. Esteves, V. M. Gaspar and J. F. Mano, *Adv. Funct. Mater.*, 2021, 31.

14 L. Zhang, H. Li, X. Lai, T. Gao and X. Zeng, *ACS Appl. Mater. Interfaces*, 2020, **12**, 44360–44370.

15 Z. Ma, H. Li, X. Jing, Y. Liu and H. Y. Mi, *Sens. Actuators, A*, 2021, **329**, 112800.

16 C. S. Luo, P. Wan, H. Yang, S. A. A. Shah and X. Chen, *Adv. Funct. Mater.*, 2017, 27.

17 T. P. Huynh, P. Sonar and H. Haick, *Adv. Mater.*, 2017, **29**, 1–14.

18 Y. J. Tan, J. Wu, H. Li and B. C. K. Tee, *ACS Appl. Mater. Interfaces*, 2018, **10**, 15331–15345.

19 S. Wang and M. W. Urban, *Nat. Rev. Mater.*, 2020, **5**, 562–583.

20 P. Chakma and D. Konkolewicz, *Angew. Chem., Int. Ed.*, 2019, **58**, 9682–9695.

21 Y. Gai, H. Li and Z. Li, *Small*, 2021, **17**, 1–19.

22 Y. Zhou, L. Li, Z. Han, Q. Li, J. He and Q. Wang, *Chem. Rev.*, 2023, **123**, 558–612.

23 S. Utrera-Barrios, R. Verdejo, M. A. López-Manchado and M. Hernández Santana, *Mater. Horiz.*, 2020, **7**, 2882–2902.

24 S. Kang, A. R. Jones, J. S. Moore, S. R. White and N. R. Sottos, *Adv. Funct. Mater.*, 2014, **24**, 2947–2956.

25 B. J. Blaiszik, A. R. Jones, N. R. Sottos and S. R. White, *J. Microencapsulation*, 2014, **31**, 350–354.

26 S. V. Wanasinghe, O. J. Dodo and D. Konkolewicz, *Angew. Chem., Int. Ed.*, 2022, **61**, e202206938.

27 L. Hammer, N. J. Van Zee and R. Nicolaÿ, *Polymers*, 2021, **13**, 396.

28 B. Zhang, N. De Alwis Watuthanthrige, S. V. Wanasinghe, S. Averick and D. Konkolewicz, *Adv. Funct. Mater.*, 2022, **32**, 2108431.

29 X. Xiao, T. Xie and Y. T. Cheng, *J. Mater. Chem.*, 2010, **20**, 3508–3514.

30 V. K. Thakur and M. R. Kessler, *Polymer*, 2015, **69**, 369–383.

31 E. B. Stopler, O. J. Dodo, A. C. Hull, K. A. Weaver, P. Chakma, R. Edelmann, L. Ranly, M. B. Zanjani, Z. Ye and D. Konkolewicz, *Mater. Adv.*, 2020, **1**, 1071–1076.

32 H. Dai, *Surf. Sci.*, 2002, **500**, 218–241.

33 D. Mai, J. Mo, S. Shan, Y. Lin and A. Zhang, *ACS Appl. Mater. Interfaces*, 2021, **13**, 49266–49278.

34 A. Peigney, C. Laurent, E. Flahaut, R. R. Bacsa and A. Rousset, *Carbon*, 2001, **39**, 507.

35 O. J. Dodo, L. Petit, D. Dunn, C. P. Myers and D. Konkolewicz, *ACS Appl. Polym. Mater.*, 2022, **4**, 6850–6862.

36 S. Iijima, *Nature*, 1991, **354**, 56–58.

37 D. Yuan, H. Guo, K. Ke and I. Manas-Zloczower, *Composites, Part A*, 2020, **132**, 105837.

38 Q. T. Li, M. J. Jiang, G. Wu, L. Chen, S. C. Chen, Y. X. Cao and Y. Z. Wang, *ACS Appl. Mater. Interfaces*, 2017, **9**, 20797–20807.

39 P. Liu, *Eur. Polym. J.*, 2005, **41**, 2693–2703.

40 N. De Alwis Watuthanthrige, D. Dunn, M. Dolan, J. L. Sparks, Z. Ye, M. B. Zanjani and D. Konkolewicz, *ACS Appl. Polym. Mater.*, 2022, **4**, 1475–1486.

41 S. J. Garcia, *Eur. Polym. J.*, 2014, **53**, 118–125.

42 N. De Alwis Watuthanthrige, P. Chakma and D. Konkolewicz, *Trends Chem.*, 2021, **3**, 231–247.

43 C.-M. Chang and Y.-L. Liu, *Carbon*, 2009, **47**, 3041–3049.

44 N. P. Truong, G. R. Jones, K. G. E. Bradford, D. Konkolewicz and A. Anastasaki, *Nat. Rev. Chem.*, 2021, **5**, 859–869.

45 G. R. Jones, A. Anastasaki, R. Whitfield, N. Engelis, E. Liarou and D. M. Haddleton, *Angew. Chem., Int. Ed.*, 2018, **57**, 10468–10482.

46 Millipore Sigma, *1,1'-(Methylenedi-4,1-phenylene)* bis maleimide *Product Specification:* **https://www.sigmaaldrich.com/US/en/product/aldrich/227463**.

47 J. Bai and Z. Shi, *ACS Appl. Mater. Interfaces*, 2017, **9**, 27213–27222.

48 Y. Chen, G. Liu, C. Wang, W. Zhang, R. W. Li and L. Wang, *Mater. Horiz.*, 2014, **1**, 489–506.

49 C. U. Pittman and G. A. Stahl, *J. Appl. Polym. Sci.*, 1981, **26**, 2403–2413.

50 A. P. King and H. Naidus, *J. Polym. Sci., Part C: Polym. Symp.*, 1969, **27**, 311–319.

51 A. Schiavi and A. Prato, *Polym. Test.*, 2017, **59**, 220–229.

52 B. Zhang, J. Ke, J. R. Vakil, S. C. Cummings, Z. A. Digby, J. L. Sparks, Z. Ye, M. B. Zanjani and D. Konkolewicz, *Polym. Chem.*, 2019, **10**, 6290–6304.

53 B. Zhang, Z. A. Digby, J. A. Flum, P. Chakma, J. M. Saul, J. L. Sparks and D. Konkolewicz, *Macromolecules*, 2016, **49**, 6871–6878.

54 L. Shuai, Z. H. Guo, P. Zhang, J. Wan, X. Pu and Z. L. Wang, *Nano Energy*, 2020, **78**, 105389.

55 S. C. Cummings, O. J. Dodo, A. C. Hull, B. Zhang, C. P. Myers, J. L. Sparks and D. Konkolewicz, *ACS Appl. Polym. Mater.*, 2020, **2**, 1108–1113.

56 Y. Ting, K. Dajiang, H. Weiyi, Y. Yunjie and W. Chaoxia, *Colloids Surf., A*, 2022, 130411.

57 Y. Wang, J. Hao, Z. Huang, G. Zheng, K. Dai, C. Liu and C. Shen, *Carbon*, 2018, **126**, 360–371.

58 M. Xu, J. Qi, F. Li and Y. Zhang, *Nanoscale*, 2018, **10**, 5264–5271.

59 J. Sun, Y. Zhao, Z. Yang, J. Shen, E. Cabrera, M. J. Lertola, W. Yang, D. Zhang, A. Benatar, J. M. Castro, D. Wu and L. J. Lee, *Nanotechnology*, 2018, **29**, 355304.

60 G. Ge, Y. Lu, X. Qu, W. Zhao, Y. Ren, W. Wang, Q. Wang, W. Huang and X. Dong, *ACS Nano*, 2020, **14**, 218–228.

61 B. Xu, F. Ye, R. Chen, X. Luo, G. Chang and R. Li, *Ceram. Int.*, 2022, **48**, 10220–10226.

62 M. Lin, Z. Zheng, L. Yang, M. Luo, L. Fu, B. Lin and C. Xu, *Adv. Mater.*, 2022, **34**, 1–13.

63 K. Zhang, J. Sun, J. Song, C. Gao, Z. Wang, C. Song, Y. Wu and Y. Liu, *ACS Appl. Mater. Interfaces*, 2020, **12**, 45306–45314.

64 M. Park, J. Park and U. Jeong, *Nano Today*, 2014, **9**, 244–260.

65 J.-S. Noh, *Polymers*, 2016, **8**, 123.

66 National Instruments, *Application Note 078*, 1998, 1–12.

67 N. Lu, X. Wang, Z. Suo and J. Vlassak, *Appl. Phys. Lett.*, 2007, **91**, 8–11.

68 S. Yang and N. Lu, *Sensors*, 2013, **13**, 8577–8594.

69 J. A. Rogers, M. G. Lagally and R. G. Nuzzo, *Nature*, 2011, **477**, 45–53.

70 Y. Gao, Y. Cheng, H. Zhang and N. Zou, *Measurement*, 2019, **139**, 380–386.

71 S. Jung, A. Sou, E. Gili and H. Sirringhaus, *Org. Electron.*, 2013, **14**, 699–702.

72 Z. Chen, W. Ren, L. Gao, B. Liu, S. Pei and H. M. Cheng, *Nat. Mater.*, 2011, **10**, 424–428.

73 B. Zhang, Z. A. Digby, J. A. Flum, E. M. Foster, J. L. Sparks and D. Konkolewicz, *Polym. Chem.*, 2015, **6**, 7368–7372.